

THE SENSITIVE STRUCTURE OF PARTIALLY PREMIXED METHANE-AIR VS. AIR COUNTERFLOW FLAMES

MICHAEL A. TANOFF AND MITCHELL D. SMOOKE

*Department of Mechanical Engineering
Yale University, P.O. Box 208284
New Haven, CT 06520-8284, USA*

ROBIN J. OSBORNE, THOMAS M. BROWN AND ROBERT W. PITZ

*Department of Mechanical Engineering
Vanderbilt University
Nashville, TN 37235, USA*

Detailed numerical calculations, which are supported experimentally, are used to investigate the sensitivity of flame structure to fuel premixedness and overall strain rate. The study covers a wide range of fuel premixedness—from $\phi = 1.3$ to $\phi = 2.0$, plus a pure diffusion flame—over a wide range of strain rates—from moderate to near extinction—in methane-air vs. air counterflow flames. The flames are observed to change drastically in structure and character—from a single, merged flame in the vicinity of the stagnation plane to a double flame consisting of a premixed-type, fuel-side flame and a stagnation-region diffusion flame—as the fuel stream equivalence ratio is perturbed slightly below $\phi \approx 1.5$ –1.4. Accordingly, the mode and amount of NO_x formation changes severely. This duality in flame structure is further discerned by monitoring the relative locations of CH and OH profiles, as these are indicators of specific flame chemistry. The exact value of the “changeover” equivalence ratio depends upon the flame’s strain rate, and in fact, flames close enough to extinction remain as a merged flame structure even at the lowest equivalence ratio. The maximum fuel-side velocity gradient is shown to be an extremely sensitive and sharp indicator of flame character, being completely insensitive to fuel-stream equivalence ratio above certain strain-dependent values, but varying sharply with equivalence ratio below these values. Other parameters, such as the width of the temperature or product species profiles, are shown to be indicators of flame structure, also, but are not nearly as sharply responsive as the fuel-side velocity gradient. These results could have important implications for design criteria for commercial burners, as well as for applications to the prediction of turbulent flame structure, including suppression and extinction.

Introduction

Residential and commercial applications of gas-fired burners (e.g., stoves, furnaces) and their associated environmental concerns have increased the need to better understand the structure and extinction characteristics of partially premixed flames. Likewise, the widely accepted laminar flamelet model of non-premixed turbulent combustion requires detailed understanding of the behavior of partially premixed flames. Furthermore, fundamental studies of flame structure (both experimental and modeling) often require classification in terms of either premixed, non-premixed, or partially premixed.

Partially premixed flames have been studied theoretically, experimentally, and numerically, with varying degrees of detail and generality. Yamaoka and Tsuji [1], using a porous cylinder burner, verified the double flame structure that occurs in some partially premixed systems. They monitored the separation

between the two observed luminous zones as a function of fuel-stream stoichiometry ($1.55 \leq \phi \leq 3.00$). Peters [2], using large activation energy asymptotics with one-step chemistry, showed that premixedness increases a flame’s sensitivity to stretch-induced extinction. Rogg, Behrendt, and Warnatz [3], using detailed numerical calculations, examined the differences in structure between a methane vs. air diffusion flame and a stoichiometric methane-air vs. air flame, two “limiting” cases of counterflow flame configuration. Smooke, Seshadri, and Puri [4] compared detailed numerical calculations against experimental measurements for one particular partially premixed system—a very rich ($\phi = 20$) jet vs. a very lean ($\phi = 0.5$) jet. Law et al. [5] developed an asymptotic theory for describing the different regimes of diluted fuel vs. partially premixed fuel counterflow flames. They showed that three flame configurations—a single, “merged” flame and two cases of a double flame—may result,

depending on the stoichiometry in the partially premixed fuel stream. And most recently, Nishioka et al. [6] used numerical calculations to study NO emissions within the partially premixed system's double-flame structure.

In this paper, we combine detailed numerical calculations with verification from laser diagnostics to study the sensitivity of counterflow flame structure to both the degree of premixedness in the (rich) fuel stream and the flame's overall strain rate. We study a wide range of premixedness—from $\phi = 1.3$ to $\phi = 2.0$, plus a pure diffusion flame—for flames burning methane in air, over a wide range of strain rates—from moderate through extinction. In addition to mapping the character of flame structure in the parametric space of fuel-side equivalence ratio and strain rate, we are interested in noting, particularly, any abrupt changes in flame structure that may occur over *narrow* ranges of stoichiometry or strain, including abrupt changes in the levels of pollutant (NO_x) formation. We present the computational approach in the next section, followed by a description of the experimental technique. Finally, the results are presented and conclusions drawn.

Computational Approach

A wide range of partially premixed counterflow flames, varying in both degree of premixedness of the fuel stream and strain rate, are simulated with the continuation code developed previously [7]. We consider a laminar counterflow flame stabilized in the vicinity of the stagnation plane between two axisymmetric, counterflowing jets separated by 1.27 cm. One jet contains the partially premixed fuel, and the other jet contains the air. The complete formulation of the mathematical model for solving the finite burner separation problem with plug flow boundary conditions is described in detail elsewhere [8,9].

Briefly, we begin with the elliptic form, in cylindrical coordinates, of the two-dimensional equations describing the conservation of total mass, individual chemical species mass, momentum, and energy for the reactive flow occurring between the two jets. To reduce the complexity of the problem, we seek a similarity solution [8] of the form

$$v = v(z), u = rU(z), Y_k = Y_k(z), T = T(z) \quad (1)$$

in which r and z are the independent radial and axial coordinates; u and v are the radial and axial components of the flow velocity; Y_k is the mass fraction of the k th chemical species; and T is the temperature. If the expressions for u and v are substituted into the continuity and momentum equations, one finds that the axial pressure gradient and the reduced radial pressure gradient are, at most, functions of z alone. A consequence of this is that the

reduced radial pressure gradient must be a constant, that is,

$$\frac{1}{r} \frac{\partial p}{\partial r} = J = \text{constant} \quad (2)$$

in which p is the pressure. This result, coupled with the similarity transformations, reduces the governing equations to a nonlinear, two-point boundary value problem in the axial (z) direction along the stagnation point streamline. These equations are discretized with an adaptive finite difference algorithm and solved using Newton's method. The system is closed with an equation of state (in this case, the ideal gas law) and appropriate boundary conditions, for which plug flow is assumed for the velocity boundaries.

In order to calculate flames with different equivalence ratios and different jet velocities (strain rates) efficiently, we employ the adaptive arc-length continuation algorithm [7,8]. This reduces the dependence of convergence on the initial estimate of the solution profiles.

It is important to note that in the preceding mathematical formulation, the governing equations do not explicitly contain the strain rate. The magnitude of the reduced pressure gradient, J , is related to the strain of the flame due to the imposed flow. Thus, as J increases, so does the strain rate, and we could use J as a measure of a characteristic strain rate. However, a more commonly accepted measure of an effective strain rate is the maximum value of the oxidizer-side velocity gradient just before the flame [9]. Furthermore, this characteristic strain rate of the inner flow may be approximated from the outer flow (jet exit conditions) according to the formula [10]

$$a = \frac{2|v_o|}{L} \left(1 + \frac{|v_f| \sqrt{\rho_f}}{|v_o| \sqrt{\rho_o}} \right) \quad (3)$$

in which a is the strain rate (s^{-1}); v_o is the oxidizer jet exit velocity; v_f is the fuel jet exit velocity; ρ_o is the oxidizer jet exit density; ρ_f is the fuel jet exit density; and L is the separation distance between the two jets. This approximate value of the characteristic strain rate is obtained easily from the experimental flow rates and boundary conditions and will be quoted in the discussion that follows.

The model employs detailed chemical kinetics and transport properties. The methane combustion mechanism includes C_2 and NO_x chemistry for 43 chemical species participating in 158 reversible chemical reactions and has been used previously in determining the structure of two-dimensional, axisymmetric laminar diffusion flames [11]. The hydrocarbon portion of the mechanism is a compilation from earlier studies [12–15], and the NO_x mechanism is that developed by Drake and Blint [16]. The chemical production rates, binary diffusion coefficients, mixture viscosity, and mixture thermal conductivity are evaluated using vectorized and highly

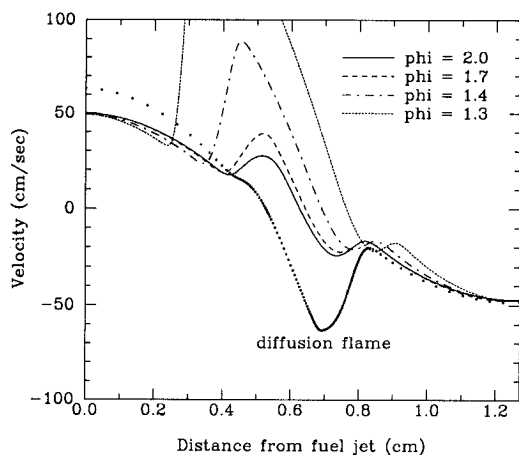


FIG. 1. Calculated velocity profiles in momentum-balanced methane-air vs. air counterflow flames. All flames have an identical strain rate of 150 s^{-1} but vary in the degree of premixedness in the fuel stream (listed as ϕ in the figure).

optimized transport and chemistry libraries [17]. The model includes thermal diffusion for light species, as well as heat losses due to radiation.

Experimental Approach

Flame structure is probed with accurate nonintrusive laser diagnostics. Measurements of major species are made by a technique based on spontaneous Raman scattering induced by a KrF excimer laser. The counterflow burner is based on a previous design [18] but with improved optical access and better exhaust gas cooling [19]. The jet separation is 1.27 cm, and the jet diameter is 2.42 cm, yielding a high aspect ratio of 1.9.

Species concentrations are measured with a narrow-band KrF excimer laser that is focused with a 200-cm lens into the reaction zone. Spontaneous Raman scattered light from CH_4 , CO_2 , CO , H_2 , O_2 , N_2 , and H_2O is collected with a Cassegrain $f/1.5$ mirror system and focused onto the entrance slit of a 0.5-m Spex spectrometer. The dispersed Raman spectrum is detected by an intensified CCD camera. The complete UV Raman system is described in detail elsewhere [19,20]. Since our techniques yield a measurement of the total number density, temperatures may be determined via the ideal gas law. For regions of the flame that exhibit polycyclic aromatic hydrocarbon fluorescence (PAH) interference, a UV sheet polarizer is placed in front of the entrance slit of the spectrometer. Measurements are taken with the polarizer at 0° , and a second set of measurements is taken with the polarizer rotated 90° . Since the Raman signals are vertically polarized and the PAH

signals are randomly polarized, a background subtraction may be made to eliminate the PAH interference in the Raman signals.

Statistical analysis of the single-shot data shows accuracy similar to that previously reported [20,21]. However, the statistical accuracy of the mean measurements is small relative to the systematic errors due to incorrect background light subtraction and errors in laser energy measurements (about ± 0.015 mole fraction). In the premixed flame region, there is increased error as a result of the additional PAH background subtraction.

Jet exit velocities are chosen so that the flames are momentum-flux balanced for each desired strain rate. That is, for a particular target strain rate desired from Eq. (3), v_f and v_o are chosen such that $\rho_f v_f^2 = \rho_o v_o^2$. We focus our experimental study on flames that range in equivalence ratio from $\phi = 1.3$ to $\phi = 2.0$, and that range in strain rates from 100 s^{-1} to 200 s^{-1} , because these are considered typical values for appliance burners.

Results and Discussion

We begin with Fig. 1, which illustrates calculated velocity profiles in a variety of flames with identical strain rates of 150 s^{-1} , but varying in the degree of premixedness in the fuel stream. Note that even some premixedness ($\phi = 2.0$) causes a deviation in character from the diffusion flame, but that the two richer flames ($\phi = 1.7$ and $\phi = 2.0$) appear to be very similar in character. However, the velocity profile in the $\phi = 1.4$ flame exhibits a markedly earlier, sharper, and stronger rise, indicating that the flame extends well into the fuel side of the stagnation plane. Compared to that of the two richer flames, in which the fuel-side velocity begins to rise approximately 2.2 mm before the stagnation plane, the fuel-side velocity in the leaner flame begins to rise 3.5 mm before the stagnation plane. This tendency is even more exaggerated in the $\phi = 1.3$ flame. Thus, at "lower" equivalence ratios, a flame exhibiting premixed character begins to establish itself on the fuel side.

It is interesting to note that the rich flammability limit for a freely propagating methane-air flame is $\phi = 1.6$ [22], an equivalence ratio straddled by the $\phi = 1.7$ and $\phi = 1.4$ profiles in Fig. 1. Thus, it may not be surprising to observe a change in flame character in the vicinity of this flammability limit in a partially premixed counterflow flame, although the flame configuration is different. However, as residence time scales decrease with increasing strain rate, this "flammability limit" may change with strain rate, also. This behavior is investigated, presently.

The calculated velocity profiles reveal the maximum fuel-side velocity gradient in the flame, and we may choose this as an indicator of the inner structure

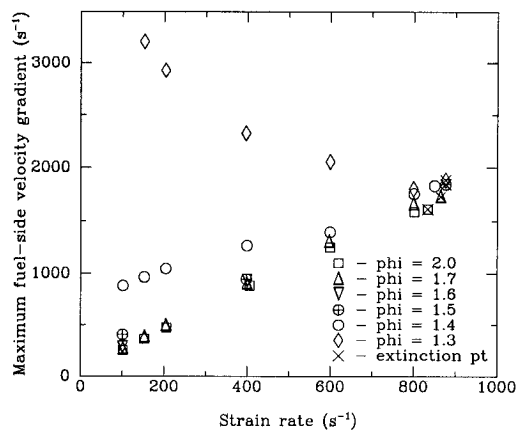


FIG. 2. Maximum fuel-side velocity gradient versus strain rate, as defined by Eq. (3), for a wide variety of fuel premixedness (listed as ϕ in the figure) in methane-air vs. air counterflow flames. Linear behavior is characteristic of a single, merged flame. Deviation from linearity indicates the onset or existence of a double-flame structure.

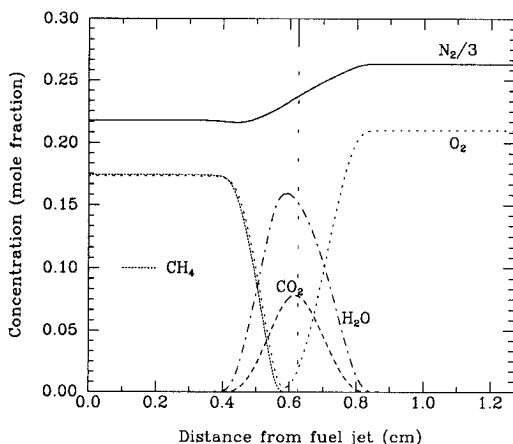


FIG. 3. Calculated major species profiles in a flame exhibiting merged flame character ($a = 150 \text{ s}^{-1}$, fuel-side $\phi = 2.0$). Note that the flame structure straddles the stagnation plane (indicated by the vertical hash marks).

of the flame. In Fig. 2, the maximum fuel-side velocity gradient is plotted against the strain rate, a , defined by Eq. 3, for a wide variation of fuel premixedness in the momentum-balanced, methane-air vs. air counterflow flames. For counterflow flames that exhibit a single-flame structure, such a plot appears linear. Figure 2 reveals this to be the case for flames having fuel-side stoichiometry $\phi \geq 1.5$ and strain rate $a \geq 150 \text{ s}^{-1}$. At $a = 100 \text{ s}^{-1}$, however, the $\phi = 1.5$ flame just begins to deviate from the linear relationship between the maximum fuel-side

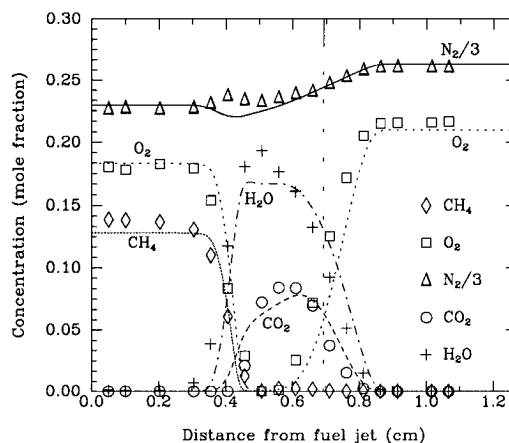


FIG. 4. Calculated (lines) and experimentally measured (symbols) major species profiles in a flame beginning to exhibit a double-flame structure ($a = 150 \text{ s}^{-1}$, fuel-side $\phi = 1.4$). Note that most of the flame structure lies to the fuel side of the stagnation plane (indicated by the vertical hash marks). Also note that model and experiment are in accord, particularly with respect to location, shape, and width of product profiles.

strain rate and a . We see, too, that the $\phi = 1.4$ case (discussed previously in relation to Fig. 1) deviates from this linear relationship for most of the range of a , but begins to approach this line at the highest strain rates. This indicates that at higher strains, a flame that could otherwise be premixed in character may not have enough time to form on the fuel side, because the fluid dynamic time scales have become too short. This may also be viewed as the "merging" of a premixed flame with a stagnation-region diffusion flame. Note that this deviation from "merged flame" behavior is quite gradual as ϕ is lowered from 1.5 to 1.4, but jumps drastically as ϕ is lowered from 1.4 to 1.3, indicating a very sensitive region for flame structure.

Major species profiles in a flame exhibiting merged flame character (fuel-side $\phi = 2.0$, $a = 150 \text{ s}^{-1}$) are illustrated in Fig. 3, and may be contrasted with the corresponding profiles for a flame that is beginning to exhibit a premixed component (fuel-side $\phi = 1.4$, $a = 150 \text{ s}^{-1}$), illustrated in Fig. 4. In the former case, the flame structure "straddles" the stagnation plane, whereas in the latter case, the majority of the flame structure lies on the fuel side of the stagnation plane. Both Figs. 3 and 4 may be contrasted against Fig. 5 in which the corresponding major species profiles are calculated for a pure diffusion flame (flame structure lies to the air side of the stagnation plane).

Figure 4 also contains results from the laser diagnostic measurements, in which model and experiment are in excellent agreement. Peak product

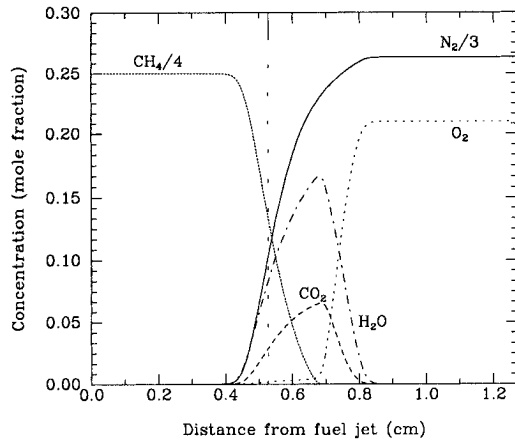


FIG. 5. Calculated major species profiles in a counterflow diffusion flame ($a = 150 \text{ s}^{-1}$). Note that the flame structure lies on the air side of the stagnation plane (indicated by the vertical hash marks).

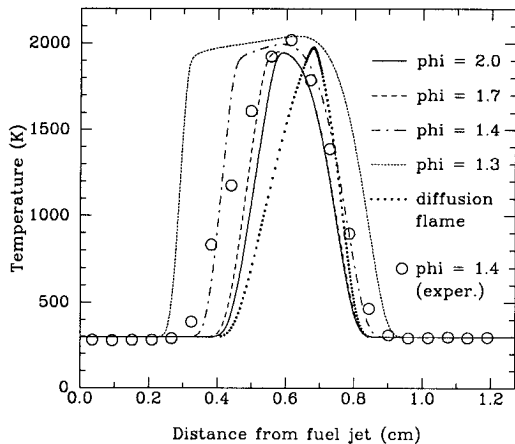


FIG. 6. Calculated temperature profiles in momentum-balanced methane-air vs. air counterflow flames. All flames have an identical strain rate of 150 s^{-1} but vary in the degree of premixedness in the fuel stream (listed as ϕ in the figure). Experimental measurements are included for the $\phi = 1.4$ case (indicated by circles in the figure).

concentrations differ slightly, but product profiles are nearly identical in location, shape, and width, which is an important comparison for the discussion that follows. We further note that model predictions and experiments are in reasonable agreement for the other experimentally investigated strain rates ($a = 100$ and 200 s^{-1}) at $\phi = 1.4$ [19].

Temperature profiles for flames with fuel premixedness $1.3 \leq \phi \leq 2.0$, as well as for a diffusion flame, are plotted in Fig. 6. As with the velocity profiles, the two richer flames exhibit very similar tempera-

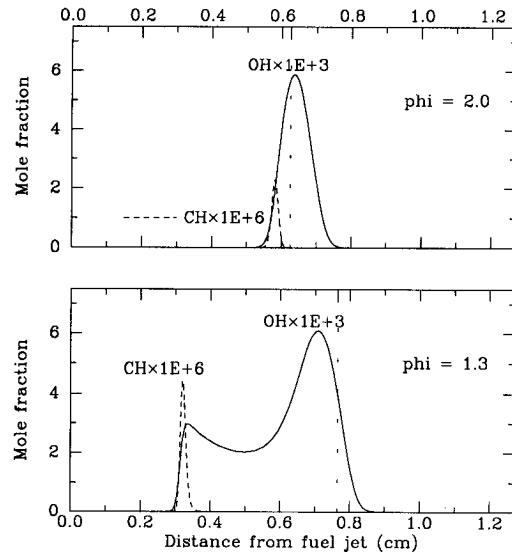


FIG. 7. Calculated CH and OH profiles in two counterflow flames with identical strain rates ($a = 150 \text{ s}^{-1}$) but with different degrees of fuel-stream premixedness (listed as ϕ in the figure). In the $\phi = 2.0$ flame, the overlapping profiles indicate a merged-flame structure in the vicinity of the stagnation plane (indicated by the vertical hash marks). The separation of the profiles in the $\phi = 1.3$ flame indicates a double-flame structure—a premixed-type flame in the partially premixed fuel stream and a diffusion flame in the vicinity of the stagnation plane.

ture profiles, and in accord with Fig. 2, the temperature profile for the $\phi = 1.4$ flame is just beginning to deviate from the two merged flame temperature profiles, whereas the temperature in the $\phi = 1.3$ flame is considerably different in character. The behavior of the $\phi = 1.4$ flame is confirmed by the Raman measurements (see Fig. 6), which are in excellent agreement with the calculations except for some temperature gradient discrepancies in the premixed region.

The merged vs. dual flame nature of these partially premixed counterflow flames may be discerned further by examining the profiles of both CH and OH. Nishioka et al. [6] cited the maxima of a rich, premixed flame and a diffusion flame, respectively, within the counterflow flame structure. Figure 7 illustrates these two species profiles for the $\phi = 2.0$ flame and the $\phi = 1.3$ flame, both at $a = 150 \text{ s}^{-1}$. The overlapping profiles in the $\phi = 2.0$ flame clearly indicate a single flame structure. This is contrasted sharply in the $\phi = 1.3$ flame. The CH peak has moved *significantly* into the fuel side of the flame and is accompanied by the lesser of *two* OH peaks. Thus, a premixed-type flame has clearly established

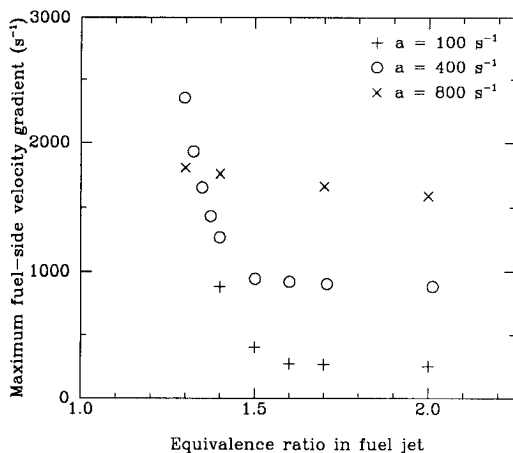


FIG. 8. Variation of maximum fuel-side velocity gradient with fuel-side equivalence ratio for three different values of flame strain rate. (Flames with $a = 800 \text{ s}^{-1}$ are very near extinction.) A rise in each data set as the equivalence ratio is lowered indicates the onset of the double-flame structure and is the region in which flame structure is extremely sensitive to the degree of fuel-stream premixedness.

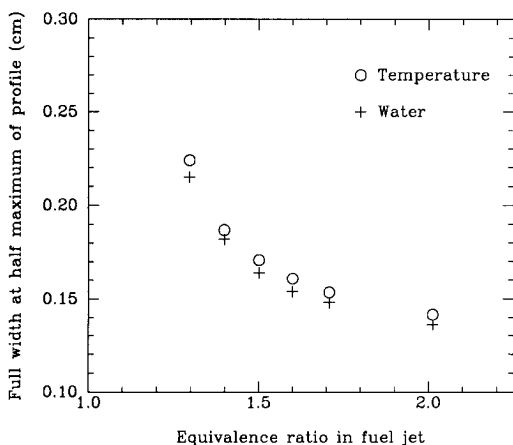


FIG. 9. Full widths at half maxima of calculated temperature and water profiles vs. fuel-side equivalence ratio for an $a = 400 \text{ s}^{-1}$ methane-air vs. air counterflow flame.

itself in the partially premixed fuel side of the counterflow system. A second, larger OH peak appears *without* an accompanying CH peak in the vicinity of the stagnation plane, indicating the location of the second (diffusion) flame, primarily due to the oxidation of CO and H₂ formed in the premixed flame.

Next, we may analyze more carefully the behavior illustrated in Fig. 2 to see how abruptly the character of a counterflow flame may change as the fuel-side

equivalence ratio is lowered. Figure 8 presents the variation of maximum fuel-side velocity gradient with ϕ for three different values of the strain rate— $a = 100, 400,$ and 800 s^{-1} . Note that the latter strain rate is just shy of extinction in all cases. The $a = 400 \text{ s}^{-1}$ plot is essentially “flat” for a fuel-side stoichiometry of $\phi \geq 1.5$ but rises *abruptly* below $\phi = 1.4$. At the lower strain rate, the flame structure is insensitive to fuel-stream stoichiometry above $\phi = 1.5$, but begins to show some sensitivity at an equivalence ratio slightly higher than in the $a = 400 \text{ s}^{-1}$ case. The near-extinction flames show no tendency for the merged flame to separate. This behavior clearly illustrates the effect of the strain-varying residence time on the rich flammability limit in the partially premixed fuel stream, lowering it considerably below the $\phi = 1.6$ value for freely propagating flames as the strain rate is increased.

The preceding discussion illustrates clearly that the maximum fuel-side velocity gradient is a viable parameter for describing the character (merged vs. dual flame) of counterflow flames. However, velocity profile measurements are not planned for our experiments, which focus on the application of Raman and laser-induced fluorescence (LIF) techniques for measuring species concentrations. Thus, another indicator of flame character would be useful—one that, perhaps, could be extracted from the species concentration measurements. A review of Figs. 4–6 suggests that the widths of either the species or the temperature profiles may, too, provide a suitable indicator of flame character. Figure 9 contains plots of the full width at half maximum of the temperature and water profiles as a function of fuel-stream equivalence ratio for counterflow flames with a fixed strain rate of $a = 400 \text{ s}^{-1}$. We see that the trend illustrated in Fig. 9 is identical to that illustrated in Fig. 8, although a definition of a single flame structure vs. a dual flame structure is not nearly as sharp.

Lastly, it is of great interest to monitor how NO_x formation varies with degree of premixedness in counterflow systems. Figure 10 illustrates NO profiles for four different fuel-side stoichiometries in a moderately strained ($a = 150 \text{ s}^{-1}$) counterflow flame. As before, the profiles from the flames that are merged structures ($\phi = 2.0, \phi = 1.7$) are very similar to each other. The NO profile is moderately different in the $\phi = 1.4$ flame as premixed character begins to appear. At $\phi = 1.3$, the flame separation is complete, and the NO profile reflects the double flame structure. Given the location of the CH peak, some of the NO present on the fuel side of the flame is generated via the Fenimore (prompt) NO_x mechanism. Conversely, the lack of any CH near the diffusion flame indicates that all of the NO present there is generated via the thermal NO_x mechanism. This observation is also consistent with the temperature profile, which barely reaches 1950 K in the

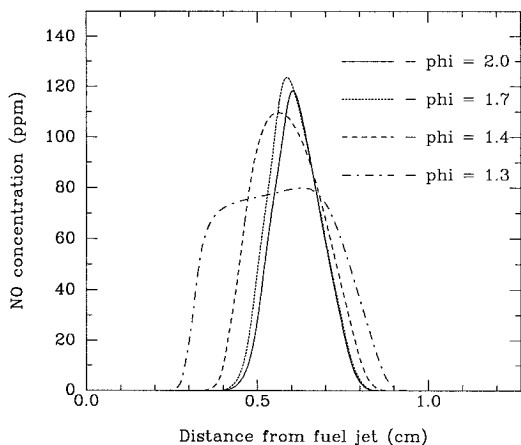


FIG. 10. Calculated NO pollutant profiles in momentum-balanced methane-air vs. air counterflow flames. All flames have an identical strain rate of 150 s^{-1} but vary in the degree of premixedness in the fuel stream (listed as ϕ in the figure).

vicinity of the CH peak but reaches a level 100 K hotter in the vicinity of the diffusion flame.

Conclusions

Partially premixed fuel-air vs. air counterflow flames change drastically in structure and character—from a single, merged flame in the vicinity of the stagnation plane to a double flame consisting of both a premixed-type, fuel-side flame and a stagnation-region diffusion flame—as the fuel-stream equivalence ratio is decreased below a strain-dependent threshold. The maximum fuel-side velocity gradient is an extremely sensitive and sharp indicator of the flame's dual character, whereas other more experimentally accessible indicators, such as the width of the temperature or product species profiles, are not nearly as sharply responsive. Experimental measurements of major species concentrations and temperature, which were taken in flames having a fuel-side stoichiometry of $\phi = 1.4$ (a stoichiometry at which separate premixed and diffusion flames are beginning to form but have not completely separated), are in very good agreement with the calculations. The change in flame structure has an extreme effect on the mode and degree of NO_x formation and could have important implications for design criteria for commercial burners, as well as for applications to the prediction of turbulent flame structure, including suppression and extinction.

Acknowledgments

Yale University gratefully acknowledges support for this research from the United States Department of Energy,

Office of Basic Energy Sciences, under grant DE-FG02-88ER13966, and from the Gas Research Institute under contract 5093-260-2807. Vanderbilt University is grateful for support from the National Science Foundation through grant CTS-9319323 and Equipment Grant CTS-9310996, and from NASA through GSRP grant NGT-1-52106.

REFERENCES

1. Yamaoka, I. and Tsuji, H., *Sixteenth Symposium (International) on Combustion*, The Combustion Institute, Pittsburgh, 1977, pp. 1145–1154.
2. Peters, N., *Twentieth Symposium (International) on Combustion*, The Combustion Institute, Pittsburgh, 1984, pp. 353–360.
3. Rogg, B., Behrendt, F., and Warnatz, J., *Twenty-First Symposium (International) on Combustion*, The Combustion Institute, Pittsburgh, 1986, pp. 1533–1541.
4. Smooke, M. D., Seshadri, K., and Puri, I. K., *Twenty-Second Symposium (International) on Combustion*, The Combustion Institute, Pittsburgh, 1988, pp. 1555–1563.
5. Law, C. K., Zhu, D. L., Li, T. X., Chung, S. H., and Kim, J. S., *Combust. Sci. Technol.* 64:199–232 (1989).
6. Nishioka, M., Nakagawa, S., Ishikawa, Y., and Takeno, T., *Combust. Flame* 98:127–138 (1994).
7. Giovangigli, V. and Smooke, M. D., *Appl. Num. Math.* 5:305–331 (1989).
8. Smooke, M. D., Crump, J., Seshadri, K., and Giovangigli, V., *Twenty-Third Symposium (International) on Combustion*, The Combustion Institute, Pittsburgh, 1990, pp. 463–470.
9. Chelliah, H. K., Law, C. K., Ueda, T., Smooke, M. D., and Williams, F. A., *Twenty-Third Symposium (International) on Combustion*, The Combustion Institute, Pittsburgh, 1990, pp. 503–511.
10. Kim, J. S., Libby, P. A., and Williams, F. A., "On the Displacement Effects of Laminar Flames," *Combust. Sci. Technol.* 87:1–25 (1992).
11. Smooke, M. D., Xu, Y., Zurn, R. M., Lin, P., Frank, J. H., and Long, M. B., *Twenty-Fourth Symposium (International) on Combustion*, The Combustion Institute, Pittsburgh, 1992, pp. 813–821.
12. Warnatz, J., *Combust. Sci. Technol.* 34:177–200 (1983).
13. Westbrook, C. K. and Dryer, F. L., *Prog. Energy Combust. Sci.* 10:1–57 (1984).
14. Miller, J. A., Kee, R. J., Smooke, M. D., and Grear, J. F., "The Computation of the Structure and Extinction Limit of a Methane-Air Stagnation Point Diffusion Flame," Paper # WSS/CI84-10, 1984 Spring Meeting of the Western States Section of the Combustion Institute, Boulder, CO, April 2–3, 1984.
15. Norton, T. S. and Smyth, K. C., *Combust. Sci. Technol.* 76:1–20 (1991).
16. Drake, M. C. and Blint, R. J., *Combust. Sci. Technol.* 75:261–285 (1991).
17. Giovangigli, V. and Darabiha, N., "Vector Computers and Complex Chemistry Combustion," in Proceedings

- of the Conference on Mathematical Modeling in Combustion, Lyon, France, NATO ASI Series, 1987.
18. Trees, D., Brown, T. M., Smooke, M. D., Seshadri, K., Balakrishnan, G., Pitz, R. W., Giovangigli, V., and Nandula, S. P., *Combust. Sci. Technol.* 104:427–439 (1995).
 19. Osborne, R. J., Brown, T. M., Pitz, R. W., Tanoff, M. A., and Smooke, M. D., "Study of Structure and Emissions of Partially Premixed Methane Flames in Laminar Counterflow," AIAA Paper No. 96-0212, 34th Aerospace Sciences Meeting and Exhibit, American Institute of Aeronautics and Astronautics, Reno, NV, 1996.
 20. Nandula, S. P., Brown, T. M., Pitz, R. W., and DeBarber, P. A., *Opt. Lett.* 19:414–416 (1994).
 21. Cheng, T. S., Wehrmeyer, J. A., and Pitz, R. W., *Combust. Flame* 91:323–345 (1992).
 22. Glassman, I., *Combustion* 2d ed., Academic Press, New York, 1987, Appendix E.

COMMENTS

R. W. Bilger, The University of Sydney, Australia. You have presented your results in terms of mole fractions versus distance with strain rate as a parameter. For diffusion flames it is more informative to plot mass fractions versus mixture fraction with the scalar dissipation at stoichiometric as a parameter. Reaction zones then appear as deviations from a straight line. Is this alternative way of presenting your data useful in this case for partially premixed flames?

Yung-cheng Chen, Tsinghua University, ROC. In your presentation, you show that the extinction of partially premixed flame can be characterized by strain rate. Also, there is only one CH zone at the fuel side reaction zone. Both suggest of a premixed-dominated flame structure at the fuel side. However, at the oxidizer side, CO/H₂ oxidation occurs at a diffusion-controlled geometry. Have you ever tried to use mixture fraction as the independent variable to analyze the flame structure at the oxidizer side instead of spatial distance?

Author's Reply. Both comments correctly suggest the utility of analyzing partially premixed counterflow flame structure in terms of mixture fraction space instead of physical space. In fact, the result of such an analysis could be quite informative in discerning differences in character between merged flame structures (e.g., fuel side $\phi = 20$), dual flame structures (e.g., fuel side $\phi = 1.3$), and "borderline" flame structures (e.g., fuel side $\phi = 1.4$, in which the merged flame is beginning to separate into a fuel side premixed-type flame and a stagnation region diffusion-type flame). As the present work focused on demonstrating how the variable flame structure may manifest itself in physical space, how sensitive it may be to the degree of fuel side premixedness, and how particular flame parameters (primarily fuel side velocity gradient) may be used in discerning flame character, such an analysis was not included in the limited space available. However, analysis in mixture fraction space is certainly planned for an expanded publication of this research, including application of such analysis to experimental results for flames exhibiting all three types of character discussed above.